

Effective interaction for charge carriers confined in quasi-one-dimensional nanostructures

S. Bednarek, B. Szafran,* T. Chwiej, and J. Adamowski
 AGH University of Science and Technology, Kraków, Poland

(Received 28 March 2003; revised manuscript received 28 May 2003; published 30 July 2003)

A problem of interacting charge carriers confined in quasi-one-dimensional (1D) semiconductor nanostructures has been studied. We have derived an analytical 1D formula for the effective interaction potential between the confined charge carriers. We have applied both the 1D model with the effective potential and the full three-dimensional (3D) approach to an electron pair confined in a single and double quantum dot as well as to an exciton confined in a quantum wire. Comparing the results of the 1D and 3D approaches we have discussed the applicability of the effective 1D interaction potential to the real 3D nanostructures. We have shown that the present effective interaction leads to accurate results for weakly coupled multiple quantum dots and wire-like nanostructures, i.e., the quantum wires and dots with the lateral confinement much stronger than the longitudinal one.

DOI: 10.1103/PhysRevB.68.045328

PACS number(s): 73.21.-b, 73.22.Gk

I. INTRODUCTION

Charge carriers in semiconductor nanostructures with a reduced dimensionality exhibit a variety of novel properties.¹ In the low-dimensional nanostructures, the confinement potential, which stems from band offsets and/or external electric fields, leads to a limitation of the motion of charge carriers in one, two, or three directions. If the confinement in two spatial directions x and y (called the lateral or transverse directions) is much stronger than the confinement in the third direction z (longitudinal direction), all the confined charge carriers occupy the lowest-energy state associated with the transverse motion, which is energetically separated from the excited states. In this case, the transverse degrees of freedom are frozen and all physically interesting effects stem from the quantized motion in the longitudinal direction. Such systems exhibit quasi-one-dimensional (1D) properties. The quasi-1D systems can be realized either in semiconductor quantum wires,¹ nano-whiskers^{2,3} or carbon nanotubes.^{4,5} The quasi-1D confinement can also be obtained in quantum dots if the lateral confinement potential is much stronger than the confinement in the growth (longitudinal) direction. The problems of charge carriers confined in quasi-1D nanostructures are of growing experimental and theoretical interest.¹⁻¹⁷ In particular, the Luttinger liquid behavior of interacting electrons in 1D medium has been reported^{4,6} and the quantization of conductance⁷ has been observed in GaAs/AlGaAs quantum wires. The ground-state energy of the 1D exciton, i.e., 1D hydrogenlike system, is divergent,¹⁸ which directly results from the singularity of the Coulomb potential at the origin. However, in the real quantum wires, which possess finite lateral extension, the exciton binding energy is finite, but grows with the strength of the lateral confinement and can be several times larger than in the bulk crystal.^{8,9} For these reasons the reduction of the original 3D problem to the effective 1D model should be performed with a special care.

The effective interaction potential for the charged particles moving in a quasi-1D medium can be derived by averaging the 3D Coulomb interaction potential over the transverse degrees of freedom.¹⁰ The correct effective potential should go over into the Coulomb potential V_C with the

asymptotic behavior $V_C \sim 1/r$ at large interparticle distances. However, instead of the Coulomb singularity at the origin, it should exhibit a cusp,¹⁰ i.e., a nonvanishing value of the first derivative. So far, this potential was calculated by a time-consuming numerical integration,^{8,19} which is not suitable for time-effective calculations in quasi-1D systems. In order to perform the effective calculations, the Coulomb potential is often replaced by approximate model potentials.^{11,20-24} The frequently used model potential energy²⁰⁻²⁴ has the following form

$$V_1(z_1 - z_2) = \frac{\kappa}{\sqrt{(z_1 - z_2)^2 + R^2}}, \quad (1)$$

where z_1 and z_2 are the longitudinal coordinates of the two charges, $\kappa = e^2/4\pi\epsilon_0\epsilon$, ϵ is the dielectric constant, and R is commonly identified with the radius of the quantum wire. This approximation correctly reproduces the asymptotic behavior at large interparticle distances, but does not lead to the cusp at zero interelectron distance. This cusp is restored by another version¹¹ of the model interaction, which has the form

$$V_2(z_1 - z_2) = \frac{\kappa}{|z_1 - z_2| + \gamma R}, \quad (2)$$

where γ is a fitting parameter.

In the present paper we have derived an analytical real-space formula (without fitting parameters) for the potential of the effective interaction between charge carriers confined in a quasi-1D environment. We have discussed the applicability of this effective potential as well as the validity of the 1D approximation for real nanostructures. For this purpose we consider a pair of electrons confined in a single and double quantum dot as well as an exciton in a quantum wire. The organization of the paper is following: in Sec. II we provide the full derivation of the effective interaction potential between the electrons in the ground state in order to allow the reader to follow our approach and to compare it with those given by other authors, Sec. III contains the results for the electron pairs and the excitons with the detailed

discussion of the applicability of the present effective potential, and Sec. IV contains the conclusions and the summary. Appendix contains the derivation of the effective interaction for higher lateral subbands.

II. EFFECTIVE TWO-PARTICLE INTERACTION POTENTIAL

First we consider a single electron moving in confinement potential U_{conf} , which can be expressed as a sum of the lateral $U_{\perp}(x,y)$ and longitudinal $U_{\parallel}(z)$ confinement potentials, i.e., $U_{\text{conf}}(x,y,z) = U_{\perp}(x,y) + U_{\parallel}(z)$. We assume that the lateral confinement is described by the harmonic oscillator potential, i.e.,

$$U_{\perp}(x,y) = \frac{1}{2}m_e\omega^2(x^2+y^2), \quad (3)$$

where m_e is the electron effective mass and ω is the harmonic oscillator frequency. The one-particle wave function for potential U_{conf} can be separated as follows:

$$\psi(\mathbf{r}) = \psi_{\perp}(x,y)\psi_{\parallel}(z), \quad (4)$$

where

$$\psi_{\perp}(x,y) = (\pi^{1/2}l)^{-1} \exp\left(-\frac{x^2+y^2}{2l^2}\right) \quad (5)$$

with the oscillator length $l = (\hbar/m_e\omega)^{1/2}$. The ground-state energy of the transverse motion is equal to $\hbar\omega$.

Let us consider two electrons confined in potential $U_{\text{conf}}(x,y,z)$. The Hamiltonian of the electron pair is given by

$$H = -\frac{\hbar^2}{2m_e}(\nabla_1^2 + \nabla_2^2) + U_{\perp}(x_1,y_1) + U_{\perp}(x_2,y_2) + U_{\parallel}(z_1) + U_{\parallel}(z_2) + \frac{\kappa}{r_{12}}, \quad (6)$$

where $r_{12} = [(x_1-x_2)^2 + (y_1-y_2)^2 + (z_1-z_2)^2]^{1/2}$. For the system of two and more charge carriers we can not separate strictly the transverse and longitudinal coordinates like in Eq. (4) because of the intrinsic inseparability of the Coulomb potential. If, however, the lateral confinement is strong, i.e., ω is large, the Coulomb interaction is a small perturbation for the transverse-motion ground state [Eq. (5)]. In this case, the following separated form

$$\Psi(\mathbf{r}_1, \mathbf{r}_2) = \psi_{\perp}(x_1, y_1)\psi_{\perp}(x_2, y_2)\Phi(z_1, z_2) \quad (7)$$

can be a good approximation of the exact two-particle wave function.

The electron-electron interaction energy can be expressed as the integral

$$W_{12} = \int d^3r_1 d^3r_2 \frac{\kappa}{r_{12}} |\Psi(\mathbf{r}_1, \mathbf{r}_2)|^2. \quad (8)$$

The Fourier transform of the lateral (transverse) probability density ψ_{\perp}^2 is given by

$$\rho_{s\perp}(k_x, k_y) = \exp[-(k_x^2 + k_y^2)l^2/4]. \quad (9)$$

We calculate integral (8) as follows. First, we replace the probability densities and the Coulomb potential by their Fourier transforms, i.e.,

$$\psi_{\perp}^2(x,y) = \frac{1}{(2\pi)^2} \int d^2k \rho_{s\perp}(k_x, k_y) \exp[-i(k_x x + k_y y)], \quad (10)$$

$$\Phi^2(z_1, z_2) = \frac{1}{(2\pi)^2} \int \int_{-\infty}^{\infty} dq_1 dq_2 \rho(q_1, q_2) \times \exp[-i(q_1 z_1 + q_2 z_2)], \quad (11)$$

and

$$\frac{1}{r_{12}} = \frac{1}{2\pi^2} \int d^2k \int_{-\infty}^{\infty} dq \frac{\exp\{-i[k_x(x_1-x_2) + k_y(y_1-y_2) + q(z_1-z_2)]\}}{k^2 + q^2}, \quad (12)$$

where $d^2k = dk_x dk_y$. Next, we integrate over \mathbf{r}_1 and \mathbf{r}_2 using the identity

$$\delta(p) = \frac{1}{2\pi} \int_{-\infty}^{\infty} dx \exp(-ipx). \quad (13)$$

The application of (13) and integration over the Dirac delta functions yields

$$W_{12} = \frac{\kappa}{2\pi^2} \int d^2k \int_{-\infty}^{\infty} dq \frac{\rho_{s\perp}^2(k_x, k_y) \rho(q, -q)}{k^2 + q^2}. \quad (14)$$

In Eq. (14) we replace $\rho(q, -q)$ by the inverse Fourier transform

$$\rho(q, -q) = \int \int_{-\infty}^{\infty} dz_1 dz_2 \Phi^2(z_1, z_2) \exp[iq(z_1 - z_2)] \quad (15)$$

and integrate over q using the identity

$$\int_{-\infty}^{\infty} dq \frac{\exp(iqz)}{k^2 + q^2} = \frac{\pi}{k} \exp(-k|z|). \quad (16)$$

The integration over k_x and k_y in Eq. (14) leads to

$$W_{12} = \int \int_{-\infty}^{\infty} dz_1 dz_2 \Phi^2(z_1, z_2) V_{\text{eff}}(z_1 - z_2), \quad (17)$$

where

$$\begin{aligned} V_{\text{eff}}(z) &= \frac{\kappa}{2\pi} \int d^2k \rho_{s\perp}^2(k_x, k_y) \frac{\exp(-k|z|)}{k} \\ &= \kappa \int_0^{\infty} dk \exp(-k|z| - k^2 l^2/2). \end{aligned} \quad (18)$$

Performing the integral in Eq. (18) we obtain the real-space form of the effective interaction potential energy

$$V_{\text{eff}}(z) = \left(\frac{\pi}{2}\right)^{1/2} \frac{\kappa}{l} \text{erfcx}\left(\frac{|z|}{2^{1/2}l}\right). \quad (19)$$

Formula (19) provides the effective potential energy of the interaction between charge carriers confined in a quasi-1D nanostructure. In Eq. (19), $\text{erfcx}(x) = \exp(x^2)\text{erfc}(x)$ is the exponentially scaled complementary error function,²⁵ which can be calculated using the standard numerical procedures (e.g., from the IMSL library²⁶). We note that the Fourier transform of the effective interaction potential (19) has been obtained by other authors^{12,27} in the following form:

$$\tilde{V}_{\text{eff}}(k) = \kappa E_1(l^2 k^2/2) \exp(l^2 k^2/2), \quad (20)$$

where E_1 is the exponential integral

$$E_1(z) = \int_z^{\infty} dx \exp(-x)/x. \quad (21)$$

However, the analytical real-space form of this potential has not been found so far. The numerical transformation of expression (20) into the real space is very cumbersome and therefore, is not suitable in the real space calculations. On the other hand, formula (19), derived in the present work, provides the analytical compact form of the effective interaction potential, which can be readily implemented in the real space calculations.

In Fig. 1 we show the comparison of effective interaction potential (19) with the Coulomb potential and model potentials (1) and (2) (cf. Sec. I). In the calculations to Fig. 1 and throughout the present paper we use the material data of GaAs, i.e., $m_e = 0.067m_{e0}$ and $\epsilon = 11$. Then, the oscillator length $l = 4.76$ nm for $\hbar\omega = 50$ meV. When plotting model potentials (1) and (2), we identify R in formulas (1) and (2) with l . Figure 1 shows that the present effective potential (19) of the interaction between the confined electrons is weaker than the Coulomb potential of the interaction between point charges for all values of the interparticle distance. At $z = 0$ effective potential (19) possesses the cusp and for $z \rightarrow \infty$ exhibits the Coulomb asymptotics. In fact, effective potential (19) becomes indistinguishable from the Coulomb potential already for $z > 25$ nm. In Fig. 1, we have also plotted effective potential (19) calculated for $\hbar\omega = 10$ meV and the same values of the other parameters. We see that for the lower value of the lateral confinement energy the effective interaction is softer at small interparticle dis-

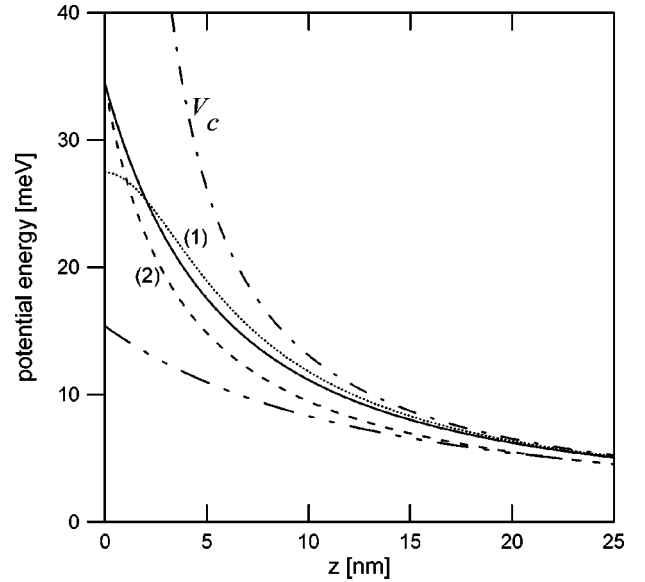


FIG. 1. Potential energy of the electron-electron interaction as a function of interelectron longitudinal distance z . The solid curve shows the present effective potential energy for the lateral confinement energy $\hbar\omega = 50$ meV, the dotted and dashed curves show model potential energies [Eq. (1)] and [Eq. (2)] both drawn for $R = l = 4.76$ nm, and the dashed-dotted curve shows the Coulomb potential energy $V_C = \kappa/z$. The dashed-double-dotted curve shows the effective interaction potential energy for $\hbar\omega = 10$ meV.

tance. Comparison of effective potential (19) with model potentials (1) and (2), presented in Fig. 1, shows that model potential (1) does not reproduce the cusp at $z = 0$. However, at large interparticle distances model potential (1), present effective potential (19), and the Coulomb potential become indistinguishable. The second model potential [cf. Eq. (2)], has been drawn for $\gamma = 0.78$, for which it reproduces the value of the effective potential (19) at the origin. Model potential (2) possesses the cusp at the origin, but in the entire range of z shown in Fig. 1 considerably underestimates both the Coulomb potential and effective potential (19). Inserting a smaller value of γ could restore the Coulomb character of model potential (2) at large interparticle distances, but it would lead to an overestimation of the electron-electron interaction energy near the origin. We conclude that none of the model potentials (1) and (2) reproduces the actual effective interaction potential in the entire range of interparticle distances.

In this section, we have obtained the real space formula for the effective interaction potential V_{eff} between the electrons occupying the lowest (s -type) subband of the quantized transverse (lateral) motion. Similar closed-form expressions can be derived for the higher lateral subbands. In Appendix we present the way one can obtain potential $V_{\text{eff}}^{\text{sp}}$ of the effective interaction between the one electron in the lowest s -type subband and the other one in the excited p -type subband.

III. APPLICATIONS

We have applied effective potential (19) to two-particle systems: a pair of electrons confined in a single and double

quantum dot and a bound electron-hole pair (exciton) in a quantum wire. We have solved the corresponding eigenvalue problems using two different approaches. The first approach [in the following called approach (I)] is based on the exact treatment of the original 3D problem followed by variational calculations with sufficiently flexible trial wave functions. When applying approach (I), we keep the 3D Coulomb interaction potential throughout the entire calculation procedure. Therefore, method (I) will provide reference results, which will be used to check the quality of the approximate 1D effective potential (19). The second approach [called approach (II)] relies on the approximate separation of the longitudinal and transverse coordinates [cf. Eq. (7)], which leads to the 1D two-particle problem with effective interaction (19). The resulting 1D Schrödinger equation for the longitudinal motion is solved numerically by the imaginary-time technique.²⁸ The comparison of the results of methods (I) and (II) allows us to study the applicability of effective interaction potential (19). In the present paper, we consider only the ground states of the two-particle systems.

A. Electron pair in a single quantum dot

First we consider a pair of electrons confined laterally by the harmonic oscillator potential [Eq. (3)]. The Hamiltonian of the system is given by Eq. (6). Due to the parabolic lateral confinement (3), it is possible to separate out the transverse center-of-mass and relative motions of electrons. The substitutions $X=x_1+x_2$, $Y=y_1+y_2$, $x_{12}=x_1-x_2$, and $y_{12}=y_1-y_2$ lead to the following separated form of Hamiltonian (6):

$$H=H_{X,Y}+H_{12}, \quad (22)$$

where Hamiltonian

$$H_{X,Y}=-\frac{\hbar^2}{m_e}\left(\frac{\partial^2}{\partial X^2}+\frac{\partial^2}{\partial Y^2}\right)+\frac{m_e\omega^2}{4}(X^2+Y^2) \quad (23)$$

has the ground state energy $\hbar\omega$, and

$$H_{12}=-\frac{\hbar^2}{2m_e}\left(2\frac{\partial^2}{\partial x_{12}^2}+2\frac{\partial^2}{\partial y_{12}^2}+\frac{\partial^2}{\partial z_1^2}+\frac{\partial^2}{\partial z_2^2}\right)+\frac{m_e\omega^2}{4}(x_{12}^2+y_{12}^2)+U_{\parallel}(z_1)+U_{\parallel}(z_2)+\frac{\kappa}{r_{12}}. \quad (24)$$

For the single quantum dot we use the Gaussian model²⁹ of the longitudinal confinement potential

$$U_{\parallel}(z)=-V_0\exp(-z^2/Z^2), \quad (25)$$

where V_0 is the depth of the potential well and Z corresponds to the range of the longitudinal confinement. The Gaussian potential was applied to a modelling of the confinement of charge carriers in both the single²⁹ and double quantum dots.^{30,31} For the Gaussian potential the one-electron eigenproblem can be solved with a high precision by both the

techniques used in the present paper, i.e., the variational method with the Gaussian basis and the imaginary time technique.

Hamiltonian (24) depends on four coordinates: the positions of both the electrons in the z direction and the relative electron-electron positions in the x - y plane. The corresponding ground-state wave function is invariant with respect to the interchange $x_{12}\leftrightarrow y_{12}$. Accordingly, the trial ground-state wave function has been taken in the form

$$\chi(x_{12},y_{12},z_1,z_2)=\sum_{ijkl}c_{ijkl}\exp[-a_iz_1^2-a_jz_2^2-b_kz_{12}^2-g_l(x_{12}^2+y_{12}^2)], \quad (26)$$

where c_{ijkl} are the linear variational parameters and a_i , a_j , b_k , and g_l are the nonlinear variational parameters. Parameters a_i and a_j describe the localization of the electrons in the Gaussian quantum dot, the term with b_k introduces the electron-electron correlation in the longitudinal direction, and g_l takes into account the dependence on the interparticle transverse distance. In the calculations, we apply four different parameters a_i , two parameters b_k , and three g_l parameters. This generates basis (26) with 96 elements, which allows us to obtain the estimates of the ground-state energy with the precision of 0.02 meV. The results obtained with method (I) with this accuracy can be treated as ‘‘exact.’’ The same precision of numerical calculations is maintained in all the implementations of methods (I) and (II) presented in the present paper.

When applying approach (II) with the effective interaction potential, we adopt the approximate separability (7) and assume that both the electrons are in the ground state of the transverse motion. We define the Hamiltonian for the longitudinal motion as operator H_{\parallel} , which fulfills the equation

$$H_{\parallel}\Phi(z_1,z_2)=\int\int\int\int_{-\infty}^{\infty}dx_1dy_1dx_2dy_2\times\psi_{\perp}(x_1,y_1)\psi_{\perp}(x_2,y_2)H\psi_{\perp}(x_1,y_1)\times\psi_{\perp}(x_2,y_2)\Phi(z_1,z_2). \quad (27)$$

Equation (27) yields

$$H_{\parallel}=-\frac{\hbar^2}{2m_e}\left(\frac{\partial^2}{\partial z_1^2}+\frac{\partial^2}{\partial z_2^2}\right)+U_{\parallel}(z_1)+U_{\parallel}(z_2)+V_{\text{eff}}(z_1-z_2)+2\hbar\omega. \quad (28)$$

The eigenvalue problem for Hamiltonian (28) depends on only two coordinates. Therefore, it can be treated with any efficient finite-difference method on a two-dimensional mesh. In the present paper, we have applied the imaginary-time technique,²⁸ according to which the ground-state wave function is calculated using the scheme $\Phi^{s+1}=(1-\alpha H_{\parallel})\Phi^s$, where s is the number of iteration. This iteration procedure converges to the exact ground-state wave function if the value of α is not too large. We have used the mesh of 400×400 grid points, for which the numerical approach

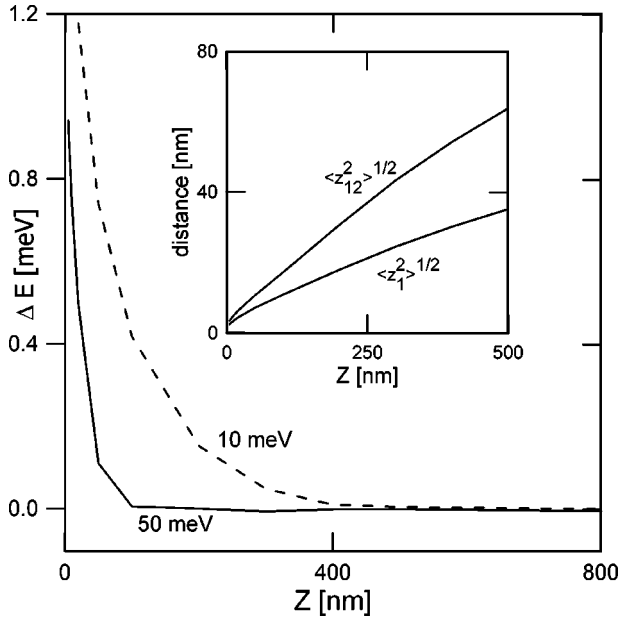


FIG. 2. Difference $\Delta E = E_{\text{II}} - E_{\text{I}}$ of the ground-state energies obtained with the effective 1D model (E_{II}) and by the full 3D approach (E_{I}) for the electron pair confined in the single quantum dot with the lateral confinement energy $\hbar\omega = 10$ meV (dashed curve) and 50 meV (solid curve) as a function of range Z of the longitudinal confinement potential. Inset, expectation values of the interelectron distance $\langle z_{12}^2 \rangle^{1/2}$ and electron-dot center distance $\langle z_1^2 \rangle^{1/2}$ as functions of Z for $\hbar\omega = 10$ meV.

works with the precision comparable to that of the variational calculations with Gaussian basis (26).

Figure 2 displays the difference $\Delta E = E_{\text{II}} - E_{\text{I}}$ between the ground-state energies calculated by methods (II) and (I) described above. The calculations have been performed for $V_0 = 200$ meV in the Gaussian confinement (25) and for the lateral confinement energy $\hbar\omega = 10$ and 50 meV. Figure 2 shows that—in the weak confinement regime, i.e., for large values of range Z of the longitudinal confinement potential—energy difference ΔE becomes equal to zero, which means that the Schrödinger equation is solved exactly in the 1D model with effective interaction potential (19) in Hamiltonian (28). In the strong confinement regime, i.e., for the small values of Z , the results obtained with Hamiltonian (28) overestimate the exact ground-state energy. This overestimation possesses a variational character. The resulting inaccuracy is related with the assumption of separability (7) and the application of the fixed form [Eq. (5)] of the wave functions, which take into account neither the electron-electron correlation nor the increase of the extension of the electron charge density in the transverse direction induced by the interelectron repulsion. For the stronger lateral confinement, i.e., for $\hbar\omega = 50$ meV, ΔE is smaller and disappears for $Z = 100$ nm, while for the weak confinement ($\hbar\omega = 10$ meV) ΔE becomes negligibly small for $Z = 300$ nm. We note that—in either case—the inaccuracy of the energy estimates is small in comparison with the ground-state energy of the two-electron system considered, which, e.g., for $\hbar\omega = 10$ meV is equal to -248.54 meV for $Z = 5$ nm and -376.22 meV for $Z = 800$ nm. Therefore, the relative accu-

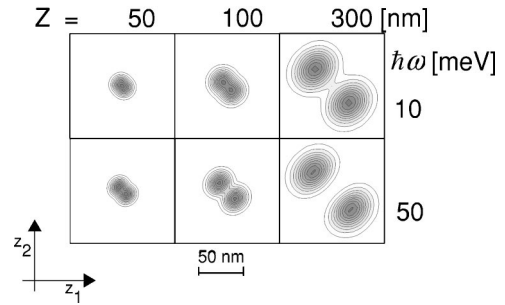


FIG. 3. Contours of the two-electron probability density for the single quantum dot as functions of the longitudinal electron coordinates z_1 and z_2 for several values of range Z of the longitudinal confinement potential and lateral confinement energy $\hbar\omega$. The bar corresponds to the length of 50 nm. The darker shade of gray corresponds to the larger probability density.

racy of the energy estimates obtained with effective potential (19) is high. Moreover, the absolute error ΔE is negligibly small as compared to the range within which the ground-state energy changes with Z .

We note that parameter Z in the Gaussian potential (25) should not be identified with the size of the quantum dot, which in fact is much smaller. The actual size of the quantum dot is illustrated in the inset of Fig. 2, which shows the average values of the electron-electron distance $\langle (z_1 - z_2)^2 \rangle^{1/2}$ and the distance of the single electron from the center of the quantum dot $\langle z_1^2 \rangle^{1/2}$ as functions of Z calculated for $\hbar\omega = 10$ meV. These average distances provide measures for the actual size of the quantum dot. For $Z = 300$ nm, for which the calculations with potential (19) are almost exact, $\langle (z_1 - z_2)^2 \rangle^{1/2} \approx 40$ nm and $\langle z_1^2 \rangle^{1/2} \approx 20$ nm.

In Fig. 3 we have plotted the contours of the two-electron probability density $\Phi^2(z_1, z_2)$ calculated by the imaginary time technique for different values of Z and $\hbar\omega$. All the plots have been drawn in the same scale (a 50 nm bar is marked in Fig. 3). In the weak confinement regime, i.e., for $Z = 300$ nm, the electrons are localized in separate regions of the quantum dot. Then, the electron density distribution has the island-like form, which means that a Wigner molecule is formed.^{21,32–35} For the larger confining frequency the Wigner molecule is created at smaller Z (cf. the plot for $\hbar\omega = 50$ meV and $Z = 100$ nm). This effect results from the fact that effective potential (19) possesses a sharper cusp at $z = 0$ for larger value of ω (cf. Fig. 1), i.e., the electron-electron repulsion, which is responsible for the formation of the Wigner molecule, is more effective. We note that the electron density for $\hbar\omega = 10$ meV and $Z = 300$ nm is very similar to that for $\hbar\omega = 50$ meV and $Z = 100$ nm. These two plots show the same shape of the two-electron probability density, i.e., one of them can be obtained from the other by a scaling. In these two cases the results obtained with the effective 1D interaction potential become indistinguishable from the 3D results for the ground-state energy (cf. Fig. 2). Both these plots correspond to the pronounced Wigner localization of the electrons. This means that the effective interaction potential, obtained in the present work, works with a high precision for the quasi-1D electron systems forming Wigner molecules.

B. Electron pair in coupled quantum dots

We have applied the effective interaction potential (19) to the problem of the electron pair confined in the coupled quantum dots.^{30,31,36–38} This system is described by Hamiltonian (6) with the longitudinal confinement potential assumed to be the double Gaussian quantum well³⁰

$$U_{||}(z) = -V_0 \{ \exp[-(z-d/2)^2/Z^2] + \exp[-(z+d/2)^2/Z^2] \}, \quad (29)$$

where d is the distance between the centers of the quantum wells.

The variational solution to the two-electron eigenproblem has been found with the use of the trial wave function expanded in the multicenter Gaussian basis

$$\chi(x_{12}, y_{12}, z_1, z_2) = \sum_{ijkl} c_{ijklmn} \exp[-a_i(z_1 - C_m)^2 - a_j(z_2 - C_n)^2 - b_k z_{12}^2 - g_l(x_{12}^2 + y_{12}^2)], \quad (30)$$

which is a generalization of wave function (26). In Eq. (30), parameters C_m and C_n stand for the z coordinates of the centers of the Gaussian functions. We have used the following four centers: $C_1 = -d/2 - Z/2$, $C_2 = -d/2$, $C_3 = d/2$, and $C_4 = d/2 + Z/2$. This choice of centers takes into account the coupling between the dots as well as the tendency of electrons to avoid one another. The introduction of the two centers per dot enables us to reduce the number of nonlinear variational parameters a_i from four in Eq. (26) to two in Eq. (30) without a significant loss of the precision. The numbers of other nonlinear parameters (b_k and g_l) are the same as in wave function (26), which generates the basis composed of 384 elements.

The results for $Z = 10$ nm are depicted as functions of interdot distance d in Fig. 4, which shows the difference $\Delta E = E_{II} - E_I$ between the ground-state energy E_{II} calculated for Hamiltonian (28) with effective potential (19) by the imaginary time technique and E_I calculated for Hamiltonian (24) with wave function (30). We see that both the energy estimates E_{II} calculated by method (II) become nearly exact for $d = 20 \div 25$ nm. Energy difference ΔE reaches zero more quickly for the stronger lateral confinement, i.e., for larger $\hbar\omega$.

The inset of Fig. 4 displays the dependence of the ground-state energy on the distance between the dot centers for $\hbar\omega = 10$ meV and for $d \in [20, 400]$ nm. The ground-state energy first grows rapidly with the interdot distance, reaches a maximum for $d = 30$ nm, and next decreases slowly. The rapid increase of the ground-state energy for small values of d is related with the decreasing overlap of the two Gaussian potential wells (29). The tunnel coupling between the dots vanishes for $d = 30$ nm. For $d > 30$ nm the electrons are localized in the different quantum dots and the electron-electron interaction energy contribution starts to decrease with the increasing interdot distance, which leads to the decreasing ground-state energy. We have found the asymptotic $1/d$ behavior of the ground-state energy (cf. inset of Fig. 4), which

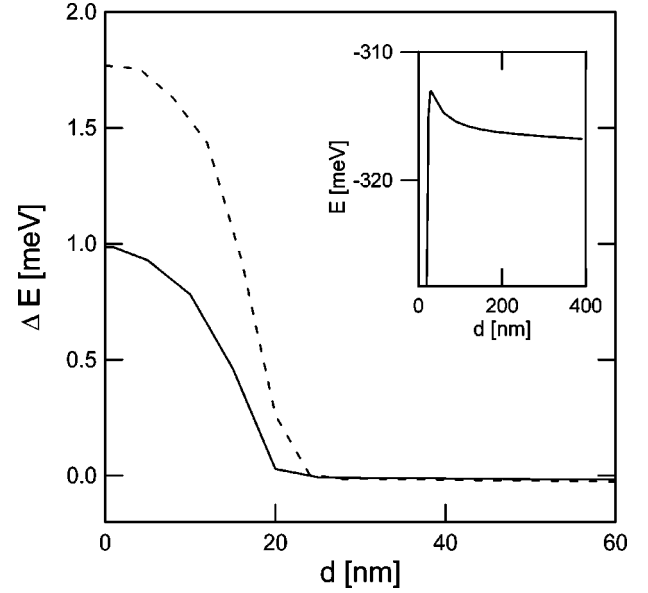


FIG. 4. Energy difference ΔE for the electron pair confined in the double quantum dot as a function of interdot distance d for the lateral confinement energy $\hbar\omega = 10$ meV (dashed curve) and 50 meV (solid curve). Inset, ground-state energy E , calculated by the full 3D approach, for the electron pair confined in the double quantum dot for $d \in [20, 400]$ nm and for $\hbar\omega = 10$ meV.

results from the Coulomb interdot repulsion, when both the electrons are localized in the different dots. Comparing the values of the total ground-state energy (inset of Fig. 4) with ΔE (Fig. 4) we see that the relative errors of method (II), which uses effective potential (19), are negligibly small. The ground-state energy is equal to -677.93 , -483.12 , and -328.46 meV for $d = 0, 12$, and 20 nm, respectively. Also the range of changes of the ground-state energy with varying d is by two orders of magnitude larger than ΔE .

In Fig. 5 we have displayed the two-electron probability density $\Phi^2(z_1, z_2)$ calculated for the coupled quantum dots by the imaginary time technique. For $d = 10$ nm confinement

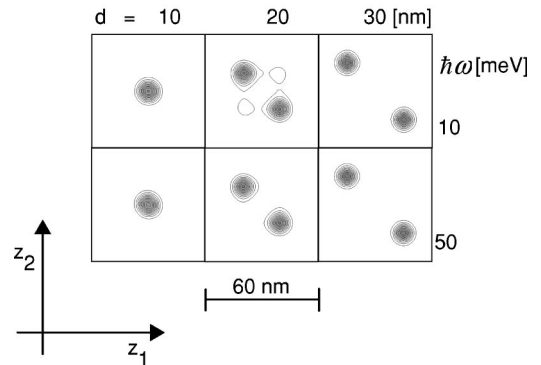


FIG. 5. Contours of the two-electron probability density for the coupled quantum dots as functions of the longitudinal electron coordinates z_1 and z_2 for several values of interdot distance d and lateral confinement energy $\hbar\omega$. The bar corresponds to the length of 60 nm. The darker shade of gray corresponds to the larger probability density.

potential (29) possesses a single minimum and the electrons are not separated spatially. The separation of the electrons becomes visible for $d=20$ nm, for which the confinement potential possesses two separated minima. The separate localization of the electrons is more pronounced for the stronger lateral confinement, i.e., for $\hbar\omega=50$ meV, than for the weaker lateral confinement, i.e., for $\hbar\omega=10$ meV, which is related to the fact that the effective interelectron repulsion (19) is stronger for the system, which is more strongly localized laterally (cf. Fig. 1). For $d=30$ nm the plots for both the lateral confinements are identical. In this case, the interaction between the electrons localized in the different dots can be identified with the electrostatic interaction between the two point charges.

C. Exciton in a quantum wire

We have also studied the applicability of the effective potential to the problem of a bound electron-hole pair in a quantum wire. In this problem the particles are free to move in the z direction. We assume the same confinement of the charge carriers in the transverse directions as in the preceding sections, i.e., parabolic lateral confinement. The system is described by the Hamiltonian

$$H = -\frac{\hbar^2}{2m_e}\nabla_e^2 - \frac{\hbar^2}{2m_h}\nabla_h^2 + \frac{m_e\omega_e^2}{2}(x_e^2 + y_e^2) + \frac{m_h\omega_h^2}{2}(x_h^2 + y_h^2) - \frac{\kappa}{r_{eh}}, \quad (31)$$

where m_h is the hole effective mass (in the calculations for the exciton we adopt $m_h=0.5m_{e0}$ and $\varepsilon=12.9$) and $r_{eh}=|\mathbf{r}_e-\mathbf{r}_h|$ is the electron-hole distance. Since the particles are not confined in the longitudinal (z) direction, we can separate in Hamiltonian (31) the center-of-mass and relative motions in this direction, which yields

$$H = -\frac{\hbar^2}{2m_e}\left(\frac{\partial^2}{\partial x_e^2} + \frac{\partial^2}{\partial y_e^2}\right) - \frac{\hbar^2}{2m_h}\left(\frac{\partial^2}{\partial x_h^2} + \frac{\partial^2}{\partial y_h^2}\right) - \frac{\hbar^2}{2M}\frac{\partial^2}{\partial Z^2} - \frac{\hbar^2}{2\mu}\frac{\partial^2}{\partial z_{eh}^2} + \frac{m_e\omega_e^2}{2}(x_e^2 + y_e^2) + \frac{m_h\omega_h^2}{2}(x_h^2 + y_h^2) - \frac{\kappa}{r_{eh}}, \quad (32)$$

where $\mu = m_e m_h / (m_e + m_h)$, $M = m_e + m_h$, $Z = (m_e z_e + m_h z_h) / M$, and $z_{eh} = z_e - z_h$. In the following, we assume that the lateral confinement for the electron and the hole is the same, i.e., $\omega_e = \omega_h = \omega$. This assumption enables us to separate the center-of-mass and relative transverse motions. We introduce the transverse coordinates for the exciton center-of-mass (c.m.) position (X and Y) and for the relative electron-hole position (x_{eh} and y_{eh}). In these coordinates, Hamiltonian (32) takes the form

$$H = H_{c.m.} + H_{eh}, \quad (33)$$

where $H_{c.m.}$ is the center-of-mass Hamiltonian with the ground-state energy $\hbar\omega$ and H_{eh} is the relative transverse-motion Hamiltonian of the form

$$H_{eh} = -\frac{\hbar^2}{2\mu}\nabla_{eh}^2 + \frac{\mu\omega^2}{2}(x_{eh}^2 + y_{eh}^2) - \frac{\kappa}{r_{eh}}. \quad (34)$$

We have calculated the ground state energy of Hamiltonian (34) using the variational wave function

$$\chi(x_{eh}, y_{eh}, z_{eh}) = \sum_{ij} c_{ij} \exp[-a_i z_{eh}^2 - b_j (x_{eh}^2 + y_{eh}^2)]. \quad (35)$$

We have applied 10 nonlinear variational parameters a_i and 10 parameters b_j , i.e., the basis set in Eq. (35) is composed of 100 elements, which leads to the sufficiently high precision of the ground-state energy estimates.

Let us introduce the effective electron-hole interaction to the problem considered. If the lateral confinement is strong, the ground-state wave function can be approximated by a product

$$\Psi(x_e, y_e, x_h, y_h, z_{eh}) = \psi_{\perp}^e(x_e, y_e) \psi_{\perp}^h(x_h, y_h) \chi_{\parallel}(z_{eh}), \quad (36)$$

where

$$\psi_{\perp}^{e(h)}(x_{e(h)}, y_{e(h)}) = (\pi^{1/2} l_{e(h)}^*)^{-1} \exp\left[-\frac{x_{e(h)}^2 + y_{e(h)}^2}{2l_{e(h)}^{*2}}\right]. \quad (37)$$

Quantities l_e^* and l_h^* are now treated as variational parameters. Similarly as in Sec. III A, we calculate the expectation value of Hamiltonian (32) by integrating over the electron and hole transverse coordinates, which yields the following one-dimensional Hamiltonian:

$$H_{\parallel} = -\frac{\hbar^2}{2\mu}\frac{d^2}{dz_{eh}^2} - V_{\text{eff}}^*(z_{eh}) + \frac{\hbar^2}{2m_e l_e^{*2}} + \frac{\hbar^2}{2m_h l_h^{*2}} + \frac{\omega^2}{2}(m_e l_e^{*2} + m_h l_h^{*2}), \quad (38)$$

where $-V_{\text{eff}}^*$ is the potential energy of the effective electron-hole interaction, which has been obtained in a similar way as the effective potential energy for the two electrons (cf. Sec. II) and has the form given by Eq. (19) with l replaced by $\sqrt{(l_e^{*2} + l_h^{*2})/2}$. We evaluate the ground-state of the exciton described by Hamiltonian (38) by a finite-difference method with a one-dimensional mesh.

In order to check the quality of the 1D approximation (38), we have calculated the ground-state energy of the exciton described by the 3D Hamiltonian (34) using trial wave function (35) and compared the results. The difference ΔE between the ground-state energy calculated by the 1D and 3D methods is displayed in Fig. 6 as a function of lateral confinement energy $\hbar\omega$.

In Fig. 6, the dashed curve has been obtained with the values of parameters l_e^* and l_h^* fixed at those for the noninteracting particles, i.e., $l_e^* = l_e$ and $l_h^* = l_h$, where $l_{e(h)} = [\hbar/m_{e(h)}\omega]^{1/2}$, and the solid curve has been obtained from the minimization performed over l_e^* and l_h^* , which significantly improved the results. We also see that the energy

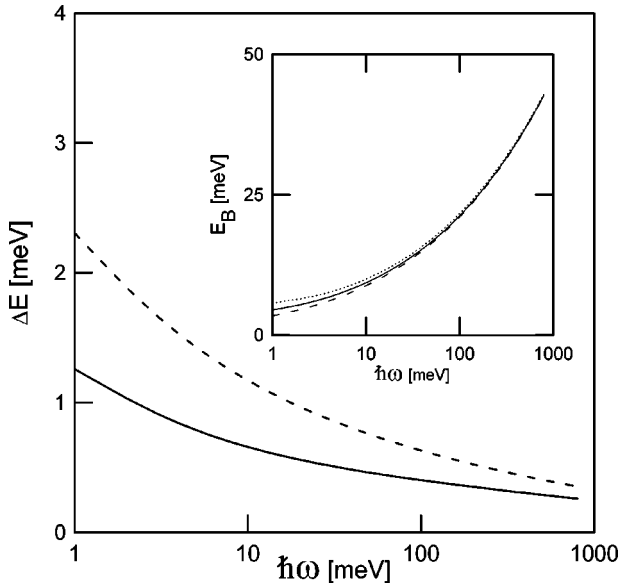


FIG. 6. Energy difference ΔE calculated for the exciton confined in the quantum wire as a function of lateral confinement energy $\hbar\omega$. The solid (dashed) curve shows the results obtained with (without) the optimization over parameters l_e^* and l_h^* in trial wave function (37). Inset, binding energy E_B of the exciton calculated with wave function (35) (dotted curve) and in the framework of the 1D model with (solid curve) and without (dashed curve) the optimization of wave function (37) as a function of lateral confinement energy $\hbar\omega$.

difference slowly decreases with the lateral confinement energy. The increasing lateral confinement energy lowers the minimal value of the effective attraction potential energy $-V_{\text{eff}}^*$ (cf. Fig. 1). As a consequence, the exciton wave function becomes more and more localized and finally resembles the Dirac delta at large $\hbar\omega$. The inset in Fig. 6 shows the binding energy E_B of the exciton, which is calculated as follows: $E_B = 2\hbar\omega - E$, where E is the exciton ground-state energy. We see that the exciton binding energy increases with increasing $\hbar\omega$, i.e., increasing confinement. The inset of Fig. 6 displays the binding energy calculated with wave function (35) and in the framework of the 1D model with and without the optimization of parameters l_e^* and l_h^* . The binding energies calculated by all the three methods become identical for the strong lateral confinement. Figure 6 also shows that ΔE , which is a measure of the accuracy of the results obtained with the effective interaction potential, becomes negligibly small for large $\hbar\omega$. The relative errors of the 1D approach with effective potential V_{eff}^* , determined with respect to the binding energy obtained with the optimized parameters l_e^* and l_h^* , have been estimated to be 22%, 7%, and 2% for $\hbar\omega = 1, 10$, and 100 meV, respectively.

IV. CONCLUSIONS AND SUMMARY

We have derived the effective potential of the interaction between the charged particles confined in the quasi-1D semiconductor nanostructure. We have considered the electron pair confined in the single and double quantum dot and the

exciton confined in the quantum wire. In order to solve the corresponding eigenvalue problems we have applied both the full 3D approach and the 1D model with the present effective interaction potential. The comparison of the results obtained by the 3D and 1D approaches enabled us to discuss the accuracy of the effective 1D model. We have shown that for the electron systems considered the present 1D model works with a reasonable precision in the entire range of the nanostructure parameters. For the single quantum dot the results of both the 3D and 1D methods become identical in the strong lateral confinement regime. For the coupled quantum dots the 1D model leads to the same results as the 3D approach at large interdot distances, i.e., if the electrons are localized in the different dots. We have also shown that the effective 1D model is suitable for a description of the exciton confined in the quantum wire.

The effective interaction potential derived in the present paper has been compared with the model interaction potentials introduced by other authors. Contrary to model potentials, the present effective potential contains no fitting parameters. At large interparticle distances both the effective and the model potentials exhibit the same coulombic asymptotics. Therefore, for the electron systems of low density the effective and model potentials should yield similar results. The differences between the effective and model potentials appear for finite interelectron distances, especially, for the very small electron-electron distance. Therefore, for the electron systems of large density, i.e., for the strong confinement, the solutions obtained with the effective and model potentials can be different. We have pointed out that the error of the energy estimates obtained with the present effective potential has a variational character and—in most cases—is negligibly small. On the contrary, the results obtained with the model potentials are non-variational, which may lead to the uncontrollable errors. These errors occur when the wave function takes on appreciable values at small interparticle distances. This problem is particularly important for the exciton confined in a quantum wire, since the electron and hole ground-state wave functions strongly overlap. In this case, the application of the model potential can yield quite arbitrary values of the binding energy. However, the application of the present effective potential leads to the reasonable values of the binding energy. If the lateral confinement potential is sufficiently strong, the ground-state energy obtained with the effective potential can be very close to the exact value, while the results obtained with the model potentials may differ significantly from the exact solutions.

In summary, we have presented the efficient method of the solution to the Schrödinger equation for the charge carriers confined in quasi-1D nanostructures. This method is based on the introduction of the effective 1D interaction potential for the charge carriers. We have derived the analytical real-space formula for the effective interaction potential, which can be readily applied to a number of problems involving quantum wires, single, and multiple quantum dots with the strong lateral confinement.

ACKNOWLEDGMENTS

This work has been supported in part by the Polish Government Scientific Research Committee (KBN).

APPENDIX

The Fourier transform of probability density $\rho_{p\perp}(x,y) = C(x^2+y^2)\exp[-(x^2+y^2)/l^2]$ of the electron in the p -type lateral subband reads

$$\begin{aligned}\rho_{p\perp}(k_x, k_y) &= \exp\left[-\frac{(k_x^2+k_y^2)l^2}{4}\right] \left[1 - \frac{l^2(k_x^2+k_y^2)}{4}\right] \\ &= \rho_{s\perp}(k_x, k_y) \left[1 - \frac{l^2(k_x^2+k_y^2)}{4}\right].\end{aligned}\quad (\text{A1})$$

We insert this Fourier transform under the integral in the effective interaction potential [Eq. (18)]

$$V_{\text{eff}}^{sp}(z) = \frac{\kappa}{2\pi} \int d^2k \rho_{p\perp}(k_x, k_y) \rho_{s\perp}(k_x, k_y) \frac{\exp(-k|z|)}{k}, \quad (\text{A2})$$

and obtain

$$\begin{aligned}V_{\text{eff}}^{sp}(z) &= \frac{\kappa}{2\pi} \left(1 - \frac{l^2}{4} \frac{\partial^2}{\partial z^2}\right) \int d^2k \\ &\times \exp\left[-\frac{(k_x^2+k_y^2)l^2}{4}\right] \frac{\exp(-k|z|)}{k},\end{aligned}\quad (\text{A3})$$

which yields

$$\begin{aligned}V_{\text{eff}}^{sp}(z) &= \frac{\kappa}{l} \left(1 - \frac{l^2}{4} \frac{\partial^2}{\partial z^2}\right) \left(\frac{\pi}{2}\right)^{1/2} \text{erfcx}\left(\frac{|z|}{2^{1/2}l}\right) \\ &= V_{\text{eff}}(z) \left(\frac{3}{4} - \frac{z^2}{4l^2}\right) + \frac{\kappa|z|}{4l^2}.\end{aligned}\quad (\text{A4})$$

This potential is softer than $V_{\text{eff}}(z)$ at $z=0$ but exhibits the same $1/z$ asymptotic behavior in the limit of large z . The corresponding formulas for the electrons occupying the other subbands can be obtained in a similar way.

*Email address: bszafran@agh.edu.pl

¹Nanotechnology, edited by G. Timp (Springer-Verlag, New York, 1999).

²B.J. Ohlsson, M.T. Björk, A.I. Persson, C. Thelander, L.R. Wallenberg, M.H. Magnusson, K. Deppert, and L. Samuelson, *Physica E (Amsterdam)* **13**, 1126 (2002).

³M.T. Björk, B.J. Ohlsson, T. Sass, A.I. Persson, C. Thelander, M.H. Magnusson, K. Deppert, L.R. Wallenberg, and L. Samuelson, *Appl. Phys. Lett.* **80**, 1058 (2002).

⁴A. Bachtold, C. Strunk, J-P. Salvetat, J-M. Bonard, L. Forro, T. Nussbaumer, and C. Schonenberger, *Nature (London)* **397**, 673 (1999).

⁵V. Derycke, R. Martel, J. Appenzellet, and P. Avouris, *Nano Lett.* **1**, 453 (2001).

⁶S. Tarucha, T. Honda, and T. Saku, *Solid State Commun.* **94**, 413 (1995).

⁷A. Yacoby, H.L. Stormer, N.S. Wingreen, L.N. Pfeiffer, K.W. Baldwin, and K.W. West, *Phys. Rev. Lett.* **77**, 4612 (1996).

⁸M.H. Szymanska, P.B. Littlewood, and R.J. Needs, *Phys. Rev. B* **63**, 205317 (2001).

⁹F. Tassone and C. Piermarocchi, *Phys. Rev. Lett.* **82**, 843 (1999).

¹⁰H. Haug and S.W. Koch, *Quantum Theory of the Optical and Electronic Properties of Semiconductors* (World Scientific, Singapore, 1994).

¹¹C. Fuchs and R.v. Baltz, *Phys. Rev. B* **63**, 085318 (2001).

¹²L. Calmels and A. Gold, *Physica E (Amsterdam)* **2**, 242 (1998).

¹³C. Gréus, L. Butov, F. Daiminger, A. Forchel, P.A. Knipp, and T.L. Reinecke, *Phys. Rev. B* **47**, 7626 (1993).

¹⁴S. Horiguchi, *Physica B* **227**, 336 (1996).

¹⁵O. Stier and D. Bimberg, *Phys. Rev. B* **55**, 7726 (1997).

¹⁶F. Perez, S. Zanier, S. Hameau, B. Jusserand, Y. Guldner, A. Cavanna, L. Ferlazzo-Manin, and B. Etienne, *Appl. Phys. Lett.* **72**, 1368 (1998).

¹⁷C. Pryor, *Phys. Rev. Lett.* **80**, 3579 (1998).

¹⁸R. Loudon, *Am. J. Phys.* **27**, 649 (1959).

¹⁹L. Banyai, I. Galbraith, C. Ell, and H. Haug, *Phys. Rev. B* **36**, 6099 (1987).

²⁰F.C. Zhang and S. Das Sarma, *Phys. Rev. B* **33**, 2903 (1986).

²¹K. Jauregui, W. Häusler, and B. Kramer, *Europhys. Lett.* **24**, 581 (1993).

²²H.J. Schulz, *Phys. Rev. Lett.* **71**, 1864 (1993).

²³M. Fabrizio, A.O. Gogolin, and S. Scheidl, *Phys. Rev. Lett.* **72**, 2235 (1994).

²⁴R. Egger and H. Grabert, *Phys. Rev. B* **55**, 9929 (1997).

²⁵Y.L. Luke, *The Special Functions and their Approximations* (Academic, New York, 1969), Vol. 1.

²⁶IMSL Fortran Library.

²⁷W.I. Friesen and B. Bergersen, *J. Phys. C* **13**, 6627 (1980).

²⁸R. Kosloff and H. Tal-Ezer, *Chem. Phys. Lett.* **127**, 223 (1986).

²⁹J. Adamowski, M. Sobkowicz, B. Szafran, and S. Bednarek, *Phys. Rev. B* **62**, 4234 (2000).

³⁰B. Szafran, S. Bednarek, and J. Adamowski, *Phys. Rev. B* **64**, 125301 (2001).

³¹J. Kolehmainen, S.M. Reimann, M. Koskinen, and M. Manninen, *Eur. Phys. J. B* **13**, 731 (2000).

³²P.A. Maksym, H. Imamura, G.P. Mallon, and H. Aoki, *J. Phys.: Condens. Matter* **12**, R299 (2000).

³³H-M. Müller and S.E. Koonin, *Phys. Rev. B* **54**, 14 532 (1996).

³⁴S.M. Reimann and M. Manninen, *Rev. Mod. Phys.* **74**, 1283 (2002).

³⁵B. Szafran, S. Bednarek, and J. Adamowski, *Phys. Rev. B* **67**, 045311 (2003).

³⁶M. Pi, A. Emperador, M. Barranco, F. Garcias, K. Muraki, S. Tarucha, and D.G. Austing, *Phys. Rev. Lett.* **87**, 066801 (2001).

³⁷B. Partoens and F.M. Peeters, *Phys. Rev. Lett.* **84**, 4433 (2000).

³⁸C. Yannouleas and U. Landman, *Eur. Phys. J. D* **16**, 373 (2001).